Hindawi
Mathematical Problems in Engineering
Volume 2019, Article ID 3451864, 17 pages
https://doi.org/10.1155/2019/3451864

Research Article

Artificial Potential Function Safety and Obstacle Avoidance Guidance for Autonomous Rendezvous and Docking with Noncooperative Target

Jianghui Liu and Haiyang Li

College of Aerospace Science and Engineering, National University of Defense Technology, Changsha, Hunan 410073, China

Correspondence should be addressed to Haiyang Li; lihaiyang@nudt.edu.cn

Received 25 April 2019; Revised 22 July 2019; Accepted 31 July 2019; Published 21 August 2019

Academic Editor: Sajad Azizi

The problem of artificial potential function (APF) safety and obstacle avoidance guidance for autonomous rendezvous and docking of chaser spacecraft with noncooperative spacecraft is studied. The relative motion equation of the chaser and the target is established based on the line-of-sight coordinate system, the reference state is designed, and the corresponding state error is deduced. The attitude motion equation of the noncooperative target spacecraft in space is established. The safety and obstacle avoidance guidance problem of autonomous rendezvous and docking with noncooperative target is transformed into a path planning problem in a dynamic environment. The attractive potential function is designed according to the state error. In order to ensure that the chaser can safely approach the noncooperative target spacecraft, a safe corridor with ellipse cissoid is designed in the final approaching stage of autonomous rendezvous and docking. The obstacle is assumed to be a sphere with a certain radius to avoid its influence in the approach, and the obstacle potential function is designed based on the Gaussian function method. The total potential function of the system is designed according to the attractive potential function, the safe potential function, and the obstacle potential function. The total potential function of the system is modified to ensure that the reference state is the minimum of the total potential function of the system. The stability of the system is proven according to the Lyapunov stability principle, and the conditions for satisfying the monotonic decrease in the total potential function of the system are deduced. Finally, the effectiveness of the proposed method is verified by three sets of numerical simulations.

1. Introduction

In recent years, with the rapid development of space technology, extensive attention has been drawn to autonomous on-orbit service technology, such as on-orbit assembly, fuel injection, component replacement, and on-orbit repair for uncontrolled spacecraft [1–6]. Compared with the cooperative target spacecraft with stable attitude in space, the uncontrolled target spacecraft generally performs free-tumbling attitude motion, showing strong noncooperative characteristics. Unlike the cooperative situations, when approaching the noncooperative target, the desired position of the chaser varies with time. To fulfill these tasks, autonomous rendezvous and docking with noncooperative target lays as the cornerstone for unmanned chaser spacecraft [7–9]. However, the space environment is complex because of space debris and accessories of noncooperative targets such as antennas, which are overwhelming obstacles for autonomous rendezvous and docking. Therefore, a guidance system is crucial to avoid collision with space debris and ensure chaser's safe approach to the noncooperative target spacecraft.

Some typical robust adaptive control methods are applied to the autonomous rendezvous and docking problem. Aiming at the measurement uncertainty and input saturation of spacecraft's rendezvous and docking, Singla et al. designed an adaptive output feedback controller [10]; Lee and Vukovich proposed a robust adaptive terminal sliding mode control with finite-time convergence [11]; Xia and Huo designed a robust adaptive backstepping neural

network controller [12]; Sun et al. proposed a robust saturation control strategy [13]; Kasaeian et al. conceived sliding mode prediction guidance method [14]; Park et al. and Zhu et al. [15, 16] proposed the model predictive control method; and Yan et al. used the inverse push scheme to design the control law [17]. Considering the total coupling uncertainty dynamics and thrust eccentricity of the rendezvous and docking process, Sun designed an adaptive sliding mode controller [18, 19]. In addition, some traditional optimization methods are also applied in this process. Harris studied the minimum rendezvous time between multiple spacecraft based on the differential drag method [20]. Boyarko et al. studied the minimum time and minimum energy optimal trajectory for the rendezvous and docking of two spacecraft in a circular orbit [21]. Oghim et al. studied the minimum velocity change and wait time for noncoplanar and general orbits to achieve optimal rendezvous [22]. Duan et al. used fuel consumption as a constraint and designed a fuel optimal controller for rendezvous and docking of noncooperative targets [23]. Ciarcià et al. designed a trajectory planner based on inverse dynamics with minimum energy as optimization objective [24]. Huang and Jia studied the finite-time rendezvous and docking problem with noncooperative targets [25]. Breger and How proposed an active safety method, which regarded the safety of rendezvous and docking process as a constraint and guaranteed safety without additional fuel consumption [26]. Jacobsen et al. used genetic algorithms to optimize the safety and fuel, and since the safety is only considered as a goal rather than a constraint, its rendezvous trajectory is actually unsafe [27].

The artificial potential function (APF) guidance method and trajectory curvature guidance method [28] show superior obstacle avoidance performance in path planning applications. The APF guidance method derived from robot path planning has the advantages of theoretically proven stability and high computational efficiency. It has successfully been applied to the spacecraft autonomous rendezvous and docking and autonomous path planning problems. Cao et al. conceived a suboptimal APF sliding mode control method [29], and Feng et al. designed a new sliding mode control strategy based on APF [30]. Dong et al. proposed a real-time adaptive control law, which introduced the potential function method to constrain the path of the chaser [31] and then drew into a special artificial potential field method based on double quaternion to constrain the track of the chaser [32]. Chen et al. used the artificial potential field method to perform on-orbit assembly of four flexible spacecraft, and the proposed control strategy can protect the chaser spacecraft against collision before reaching the desired position [33]. Bloise designed the obstacle avoidance guidance algorithm by combining artificial potential field theory with sliding mode technology [34]. In terms of safety research on rendezvous and docking with noncooperative target, Zhang et al. concentrated on obstacle avoidance using artificial potential field guidance [35].

However, the above research is not without flaws. First, most relative motion equations are based on the circular orbits of the Clohessy–Wiltshire (CW) equation, and the relative motion between spacecraft is described by the orbital coordinate system, which requires high-precision telemetry and filtering on the ground. Those methods often result in poor real-time performance and large position error. Secondly, the relevant research focuses more on the cooperative target but less on the noncooperative target. Besides, risky debris as the cause of collisions in the space is often ignored since research concerning rendezvous and docking safety centers on avoiding collisions with the accessories of the target.

Therefore, based on the above considerations, the relative motion equation is established in line-of-sight coordinate system in this paper, which is applicable to any orbit. The relative motion between the chaser and the target mainly depends on the sensor of the chaser itself, which delivers better real-time performance and smaller position error. Secondly, the method proposed in this paper is aimed at noncooperative target and is more widely used. Finally, the method proposed here can not only achieve safe rendezvous and docking but also avoid the influence of space debris.

The rest sections are as follows: Section 2 introduces the relative motion equation between the chaser and the target and deduces the attitude motion equation of the target. Section 3 establishes the attractive potential function, the safe potential function, and the obstacle potential function, respectively. The time derivative of each potential function is deduced, and the total potential function of the system is established and modified. The stability of the system is analyzed by using Lyapunov theory, and the control acceleration of the chaser is deduced in Section 4. Simulation studies performed on autonomous rendezvous and docking with noncooperative target are presented in Section 5. Section 6 draws conclusions.

2. Relative Dynamics and Attitude Motion

2.1. Relative Dynamics. The relative motion between the chaser and the target is shown in Figure 1, where $\mathscr{F}_{\mathrm{I}} = \{o_{\mathrm{I}} x_{\mathrm{I}} y_{\mathrm{I}} z_{\mathrm{I}}\}$ is the Earth-centered inertial coordinate system, $\mathscr{F}_{\mathrm{S}} = \{o_{\mathrm{S}} x_{\mathrm{S}} y_{\mathrm{S}} z_{\mathrm{S}}\}$ is the line-of-sight coordinate system, and $\mathscr{F}_{\mathrm{B}} = \{o_{\mathrm{B}} x_{\mathrm{B}} y_{\mathrm{B}} z_{\mathrm{B}}\}$ is the body coordinate system of the target. $\mathbf{r}_c^{\mathrm{I}} \in \mathbb{R}^3$ and $\mathbf{r}_t^{\mathrm{I}} \in \mathbb{R}^3$ are the position vectors of the chaser's centroid and target's centroid in the frame $\mathscr{F}_{\mathrm{I}}$, respectively. $\mathbf{r}_{ct}^{\mathrm{I}} = [x_{ct}^{\mathrm{I}}, y_{ct}^{\mathrm{I}}, z_{ct}^{\mathrm{I}}]^T$ is the position vector of the target relative chaser described in the frame $\mathscr{F}_{\mathrm{I}}$, and the relative distance between the two spacecraft is $r = \|\mathbf{r}_{ct}^{\mathrm{I}}\|$. $q_\varepsilon \in (-\pi/2, \pi/2)$ is the azimuth angle, $q_\beta \in (-\pi, \pi)$ is the altitude angle, and $q_\varepsilon \in \mathbb{R}$ and $q_\beta \in \mathbb{R}$ are collectively referred to as position angles.

The relative motion equation between two spacecraft described in the frame $\mathscr{F}_{\mathrm{S}}$ is [36]

$$\begin{cases} \ddot{r} - r\left(\dot{q}_\varepsilon^2 + \dot{q}_\beta^2 \cos^2 q_\varepsilon\right) = a_{tx} - a_{cx} + \Delta a_x, \\ r\ddot{q}_\varepsilon^2 + 2\dot{r}\dot{q}_\varepsilon + r\dot{q}_\beta^2 \sin q_\varepsilon \cos q_\varepsilon = a_{ty} - a_{cy} + \Delta a_y, \\ -r\ddot{q}_\beta \cos q_\varepsilon + 2r\dot{q}_\varepsilon\dot{q}_\beta \sin q_\varepsilon - 2\dot{r}\dot{q}_\beta \cos q_\varepsilon = a_{tz} - a_{cz} + \Delta a_z, \end{cases} \tag{1}$$

where $[a_{tx}, a_{ty}, a_{tz}]^T$ and $[a_{cx}, a_{cy}, a_{cz}]^T$ are the acceleration vectors of the target and the chaser in the frame $\mathscr{F}_{\mathrm{I}}$,

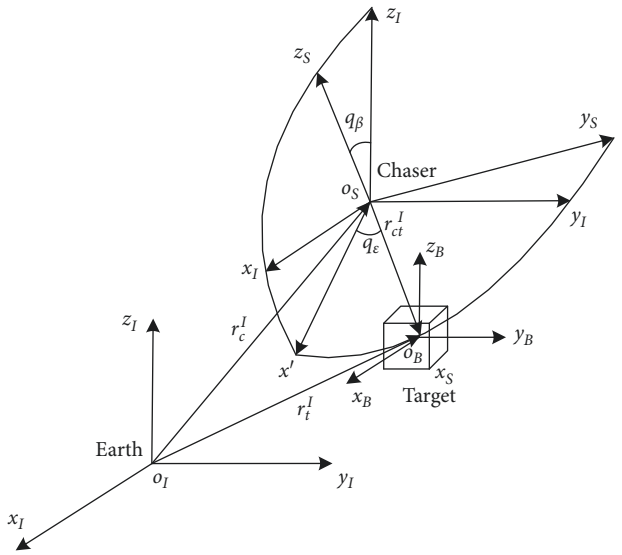

Figure 1: Relative motion coordinate system.

respectively. $[\Delta a_x, \Delta a_y, \Delta a_z]^T$ is the gravitational difference between the two spacecraft. When $r \in \mathbb{R}$ is small, $[\Delta a_x, \Delta a_y, \Delta a_z]^T$ can be ignored. It can be seen from equation (1) that the relative motion equation is only related to the relative position r, the azimuth angle q_ε, and the altitude angle q_β and is independent of the target's orbit, so the relative motion equation is applicable to any orbit. The attitude transfer matrix from the frame F_I to the frame $\mathscr{F}_\mathrm{S}$ is $\mathbf{M}_\mathrm{I}^\mathrm{S} \in \mathbb{R}^{3\times3}$, and its expression is

$$\mathbf{M}_\mathrm{I}^\mathrm{S} = \begin{bmatrix} \cos q_\varepsilon \cos q_\beta & \sin q_\varepsilon & -\cos q_\varepsilon \sin q_\beta \\ -\sin q_\varepsilon \cos q_\beta & \cos q_\varepsilon & \sin q_\varepsilon \sin q_\beta \\ \sin q_\beta & 0 & \cos q_\beta \end{bmatrix}. \tag{2}$$

Equation (1) shows that there is a strong coupling between $r \in \mathbb{R}$ and $\cos q_\varepsilon$, and both $r \in \mathbb{R}$ and $\cos q_\varepsilon$ are positive numbers. The state variables are defined as $x_1 = r$, $x_2 = q_\varepsilon$, $x_3 = q_\beta$, $x_4 = \dot{r}$, $x_5 = r\dot{q}_\varepsilon$, and $x_6 = r\dot{q}_\beta \cos q_\varepsilon$. Then, equation (1) yields

$$\begin{cases} \dot{x}_1 = x_4, \\ \dot{x}_2 = \dfrac{x_5}{x_1}, \\ \dot{x}_3 = \dfrac{x_6}{(x_1 \cos x_2)}, \\ \dot{x}_4 = \dfrac{(x_5^2 + x_6^2)}{x_1 + a_{tx} - a_{cx} + \Delta a_x}, \\ \dot{x}_5 = \dfrac{-x_4 x_5}{x_1} - \dfrac{x_6^2 \sin x_2}{(x_1 \cos x_2) + a_{ty} - a_{cy} + \Delta a_y}, \\ \dot{x}_6 = \dfrac{-x_4 x_6}{x_1} + \dfrac{x_5 x_6 \sin x_2}{(x_1 \cos x_2) - a_{tz} + a_{cz} - \Delta a_z}. \end{cases} \tag{3}$$

The reference values of relative distance and position angle are set as r_d, $q_{\varepsilon d}$, $q_{\beta d}$, $\dot{r}_d$, $\dot{q}_{\varepsilon d}$, and $\dot{q}_{\beta d}$. Then, the error variables can be defined as

$$e_1 = r - r_d = x_1 - r_d, \tag{4a}$$

$$e_2 = q_\varepsilon - q_{\varepsilon d} = x_2 - q_{\varepsilon d}, \tag{4b}$$

$$e_3 = q_\beta - q_{\beta d} = x_3 - q_{\beta d}, \tag{4c}$$

$$e_4 = \dot{r} - \dot{r}_d = x_4 - \dot{r}_d, \tag{4d}$$

$$e_5 = r\left(\dot{q}_\varepsilon - \dot{q}_{\varepsilon d}\right) = x_5 - x_1 \dot{q}_{\varepsilon d}, \tag{4e}$$

$$e_6 = r\left(\dot{q}_\beta - \dot{q}_{\beta d}\right)\cos q_\varepsilon = x_6 - x_1 \dot{q}_{\beta d} \cos x_2. \tag{4f}$$

The error vectors are set as $\mathbf{e}_p = [e_1, e_2, e_3]^T$ and $\mathbf{e}_v = [e_4, e_5, e_6]^T$. The current state are $\mathbf{x}_p = [x_1, x_2, x_3]^T$ and $\mathbf{x}_v = [x_4, x_5, x_6]^T$, and the reference state is $\mathbf{x}_{pd} = [r_d, q_{\varepsilon d}, q_{\beta d}]^T$. Then, the following expression can be obtained:

$$\mathbf{e}_p = \mathbf{x}_p - \mathbf{x}_{pd}, \tag{5}$$

$$\mathbf{e}_v = \left[x_4 - \dot{r}_d, x_5 - x_1 \dot{q}_{\varepsilon d}, x_6 - x_1 \dot{q}_{\beta d} \cos x_2\right]^T. \tag{6}$$

The time derivatives of equations (5) and (6) give

$$\dot{\mathbf{e}}_p = \mathbf{P}_1(x)\mathbf{e}_v, \tag{7}$$

$$\dot{\mathbf{e}}_v = \dot{\mathbf{x}}_v - \mathbf{P}_2(x), \tag{8}$$

where

$$\mathbf{P}_1(x) = \mathrm{diag}\left(1, \frac{1}{x_1}, \frac{1}{(x_1 \cos x_2)}\right),$$

$$\mathbf{P}_2(x) = \begin{bmatrix} \ddot{r}_d \\ \dot{x}_1 \dot{q}_{\varepsilon d} + x_1 \ddot{q}_{\varepsilon d} \\ \dot{x}_1 \dot{q}_{\beta d} \cos x_2 - x_1 x_2 \dot{q}_{\beta d} \sin x_2 + x_1 \ddot{q}_{\beta d} \cos x_2 \end{bmatrix}. \tag{9}$$

2.2. Attitude Motion. The attitude motion model of the frame $\mathscr{F}_\mathrm{B}$ relative to the frame $\mathscr{F}_\mathrm{I}$ of the uncontrolled tumbling target spacecraft under the condition of no external torque is [11]

$$\mathbf{J}_t \dot{\omega}_\mathrm{B} + S(\boldsymbol{\omega}_\mathrm{B})\mathbf{J}_t \boldsymbol{\omega}_\mathrm{B} = 0, \tag{10}$$

where $\mathbf{J}_t \in \mathbb{R}^{3\times3}$ is the inertial matrix of target and $\boldsymbol{\omega}_\mathrm{B} \in \mathbb{R}^3$ is the angular velocity vector of the target in the frame $\mathscr{F}_\mathrm{B}$. $S(\cdot)$ represents the skew-symmetric matrix of the vector's cross multiplication. In this paper, for any vector $\boldsymbol{\xi} = [\xi_1, \xi_2, \xi_3]^+$, there is

$$S(\boldsymbol{\xi}) = \begin{bmatrix} 0 & -\xi_3 & \xi_2 \\ \xi_3 & 0 & -\xi_1 \\ -\xi_2 & \xi_1 & 0 \end{bmatrix}^T. \tag{11}$$

In order to facilitate the analysis, the quaternion is used to describe the attitude of spacecraft. The attitude kinematics equation described by the quaternion is

$$\dot{q} = \frac{1}{2} \begin{bmatrix} 0 & -\boldsymbol{\omega}_{\mathrm{B}}^T \\ \boldsymbol{\omega}_{\mathrm{B}} & -S(\boldsymbol{\omega}_{\mathrm{B}}) \end{bmatrix} \mathbf{q}, \tag{12}$$

where $\mathbf{q} = [q_0, \overline{q}^T]^T$ and $\overline{q} = [q_1, q_2, q_3]^T$. The attitude transfer matrix $\mathbf{M}_{\mathrm{I}}^{\mathrm{B}} \in \mathbb{R}^{3\times3}$ from the frame $\mathscr{F}_{\mathrm{I}}$ to the frame $\mathscr{F}_{\mathrm{B}}$ is

$$\mathbf{M}_{\mathrm{I}}^{\mathrm{B}}(\mathbf{q}) = \begin{bmatrix} q_0^2 + q_1^2 - q_2^2 - q_3^2 & 2q_1q_2 + 2q_0q_3 & 2q_1q_3 - 2q_0q_2 \\ 2q_1q_2 - 2q_0q_3 & q_0^2 - q_1^2 + q_2^2 - q_3^2 & 2q_0q_1 + 2q_2q_3 \\ 2q_1q_3 + 2q_0q_2 & 2q_2q_3 - 2q_0q_1 & q_0^2 - q_1^2 - q_2^2 + q_3^2 \end{bmatrix}. \tag{13}$$

The docking position is $\mathbf{D}_{\mathrm{B}} \in \mathbb{R}^3$ in the frame $\mathscr{F}_{\mathrm{B}}$, and then the desired position $\mathbf{D}_{Cd} \in \mathbb{R}^3$ of chaser in the frame $\mathscr{F}_{\mathrm{I}}$ is

$$\mathbf{D}_{Cd} = \left(\mathbf{M}_I^{\mathrm{B}}(\mathbf{q})\right)^{-1} \cdot (-\mathbf{D}_{\mathrm{B}}). \tag{14}$$

Since the target is in an uncontrolled tumbling state in space, the desired position $\mathbf{D}_{Cd}$ is continuously changing, and the $q_{\varepsilon d}$, $q_{\beta d}$, $\dot{q}_{\varepsilon d}$, and $\dot{q}_{\beta d}$ are also continuously changing.

3. Artificial Potential Function

The artificial potential function (APF) developed in recent years was originally used for path planning of robots. APF has theoretically been proven of its stability and high computational efficiency [37, 38], which can be applied to path planning of autonomous rendezvous and docking process [28–34]. The principle of APF guidance is to define an APF reflecting global motion of the chaser. In this paper, the APF is the total potential function of the system, which is composed of the attractive potential function, the safe potential function, and the obstacle potential function. Represented by the attractive potential function, the reference position applies gravity to the chaser. The APF has a global minimum at the reference position. Represented by the safe potential function, the safe corridor exerts repulsive force on the chaser. The obstacle potential function is used to represent the obstacle exerting repulsive force on the chaser. Safe corridor and obstacles constitute the path restricted area of the chaser. The APF has a global large value in the path restricted area. The Lyapunov stability theory is used to analyze the APF, and the appropriate control law is found to be guaranteeing the time derivative of the APF is negative, thus keeping the APF monotonously decreasing. The chaser can be ensured to effectively avoid the path restricted area while reaching the reference position, thus achieving the desired guidance.

3.1. Attractive Potential Function. The attractive potential function representing reference position is designed as

$$\Omega_d = \frac{1}{2}\mathbf{e}_p^T\mathbf{Q}_p\mathbf{e}_p + \frac{1}{2}\mathbf{e}_v^T\mathbf{Q}_v\mathbf{e}_v, \tag{15}$$

where $\mathbf{Q}_p \in \mathbb{R}^{3\times3}$ and $\mathbf{Q}_v \in \mathbb{R}^{3\times3}$ are positive definite symmetric matrices. Equation (15) shows that when $\mathbf{e}_p = \mathbf{0}$ and $\mathbf{e}_v = \mathbf{0}$, $\Omega_d = 0$, otherwise $\Omega_d > 0$. The reference position ($\mathbf{e}_p = \mathbf{0}$ and $\mathbf{e}_v = \mathbf{0}$) is the minimum value of the attractive potential function.

3.2. Safe Potential Function. During autonomous rendezvous and docking with noncooperative targets, the chaser must avoid colliding with accessories such as solar sails and antennas. Therefore, it is necessary to construct a safe corridor to restrict the chaser's path to the entire corridor. In this paper, the safe corridor is defined as the conical interior formed by rotating around the docking axis of the target at a safe angle $\varphi_{\mathrm{s}} \in (0, \pi/2)$. Within the safe distance of the target, the angle between the chaser's line-of-sight and the docking axis of the target must satisfy the following condition:

$$\alpha \le \varphi_{\mathrm{s}}. \tag{16}$$

In order to leave a safe margin, the elliptical cissoid surface rotated by the elliptical vine curve shown in Figure 2 around the docking axis of the target is used as the path restricted of the chaser during the rendezvous and docking process. The elliptic vine curve equation is as follows:

$$y^2 = \frac{x^3(\tan^2\varphi)}{2\rho - x}, \tag{17}$$

where $\rho \in \mathbb{R}$ can be considered as the representation of the safe distance, while φ represents the safe angle. In order to facilitate the analysis, the x-axis of the frame $\mathscr{F}_{\mathrm{B}}$ is used as the docking axis. The elliptical cissoid surface is obtained by rotating the elliptical vine curve around the x-axis, and the inside of the surface is the safe corridor. As shown in Figure 3, the surface equation is

$$f(x, y, z) = y^2 + z^2 - \frac{x^3(\tan^2\varphi)}{2\rho - x}. \tag{18}$$

The Gaussian function is used to represent the path restriction area. Therefore, the expression of the safe potential function Ω_{s0} based on the elliptical cissoid surface is [39]

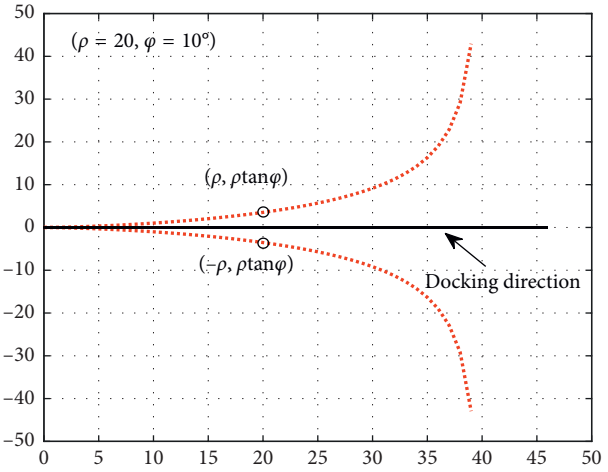

Figure 2: Elliptical vine curve.

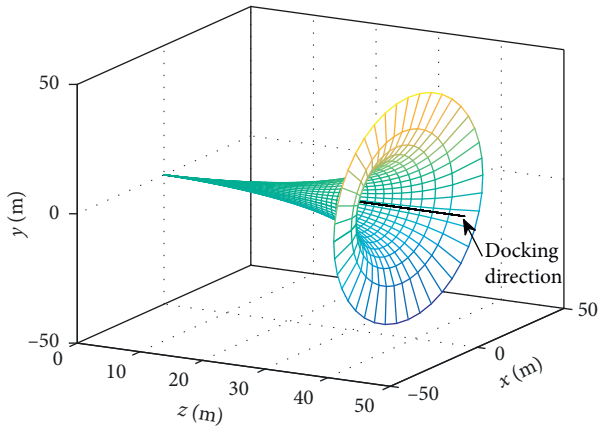

Figure 3: Elliptical cissoid surface.

$$\Omega_{s0} = k_{1s} \exp\left(-\frac{1}{2k_{2s}^2}\left|f\left(\mathbf{r}_{tc}^{\mathrm{B}}\right)\right|\right), \tag{19}$$

where $k_{1s} > 0$ indicates the height of the Gaussian function and $k_{2s} > 0$ indicates the width of the Gaussian function. $\mathbf{r}_{tc}^{\mathrm{B}} = [x_{tc}^{\mathrm{B}}, y_{tc}^{\mathrm{B}}, z_{tc}^{\mathrm{B}}]^T$ is the position vector of the chaser relative to the target described in the frame $\mathcal{F}_{\mathrm{B}}$, and the expression of $\mathbf{r}_{tc}^{\mathrm{B}} \in \mathbb{R}^3$ is

$$\mathbf{r}_{tc}^{\mathrm{B}} = -\mathbf{M}_I^{\mathrm{B}}(\mathbf{q}) \cdot \mathbf{r}_{ct}^{\mathrm{I}}. \tag{20}$$

Since the attitude $\mathbf{q} \in \mathbb{R}^4$ of the target is continuously changing, the safe corridor surface fixed to the target is also continuously changing, which is a dynamic safe corridor. At the same time, $\mathbf{r}_{tc}^{\mathrm{B}} \in \mathbb{R}^3$ changes with the change in $\mathbf{r}_{ct}^{\mathrm{I}} \in \mathbb{R}^3$. As can be seen from equation (19), when the chaser is away from the curved surface, $|f(\mathbf{r}_{tc}^{\mathrm{B}})|$ is larger and Ω_{s0} is smaller. When the chaser approaches the surface, $|f(\mathbf{r}_{tc}^{\mathrm{B}})|$ is smaller and Ω_{s0} is larger. The appropriate k_{1s} is set to ensure that the chaser is constrained to move inside the curved surface to satisfy the requirements of safe rendezvous and docking.

The time derivative of equation (19) gives

$$\dot{\Omega}_{s0}(\mathbf{q}, \mathbf{x}_p) = \Omega_{s0}(\mathbf{q}, \mathbf{x}_p) \cdot \left(-\frac{1}{2k_{2s}^2}\right) \frac{\partial\left|f\left(\mathbf{r}_{tc}^{\mathrm{B}}\right)\right|}{\partial\left(\left(\mathbf{r}_{tc}^{\mathrm{B}}\right)^T\right)} \cdot \left(\frac{\partial \mathbf{r}_{tc}^{\mathrm{B}}}{\partial \mathbf{r}_{ct}^T} \frac{\partial \mathbf{r}_{ct}}{\partial \mathbf{x}_p^T} \frac{\partial \mathbf{x}_p}{\partial t} + \frac{\partial \mathbf{r}_{tc}^{\mathrm{B}}}{\partial \mathbf{q}^T} \frac{\partial \mathbf{q}}{\partial t}\right). \tag{21}$$

Since the design requires that the chaser cannot pass through the point of the highest safe potential function, i.e., $f(\mathbf{r}_{tc}^{\mathrm{B}}) \neq 0$ is required, when calculating the time derivative of the potential function Ω_{s0} in equation (19), $f(\mathbf{r}_{tc}^{\mathrm{B}})$ cannot take absolute value, i.e.,

$$\frac{\partial\left|f\left(\mathbf{r}_{tc}^{\mathrm{B}}\right)\right|}{\partial\left(\left(\mathbf{r}_{tc}^{\mathrm{B}}\right)^T\right)} = \frac{\partial\left(f\left(\mathbf{r}_{tc}^{\mathrm{B}}\right)\right)}{\partial\left(\left(\mathbf{r}_{tc}^{\mathrm{B}}\right)^T\right)} = \left[-\frac{2\left(x_{tc}^{\mathrm{B}}\right)^2 \cdot \left(3\rho - x_{tc}^{\mathrm{B}}\right)\tan^2\varphi}{\left(2\rho - x_{tc}^{\mathrm{B}}\right)^2}, 2y_{tc}^{\mathrm{B}}, 2z_{tc}^{\mathrm{B}}\right]. \tag{22}$$

The other partial time derivatives in equation (21) are solved as follows:

$$\frac{\partial \mathbf{r}_{tc}^{\mathrm{B}}}{\partial \mathbf{r}_{ct}^{T}} = -\mathbf{M}_{I}^{\mathrm{B}}(\mathbf{q}) \cdot \mathrm{diag}(1,1,1) = -\mathbf{M}_{I}^{\mathrm{B}}(\mathbf{q}). \tag{23}$$

$\mathbf{r}_{ct}^{\mathrm{I}} = (\mathbf{M}_{\mathrm{I}}^{\mathrm{S}})^{T}\mathbf{r}_{ct}^{\mathrm{S}}$ and $\mathbf{r}_{ct}^{\mathrm{S}} = [r,0,0]^{T}$ yield

$$\begin{aligned}
\mathbf{r}_{ct}^{\mathrm{I}} &= \left[r\cos q_{\varepsilon}\cos q_{\beta}, r\sin q_{\varepsilon}, -r\cos q_{\varepsilon}\sin q_{\beta}\right]^{T},\\
\frac{\partial \mathbf{r}_{ct}^{\mathrm{I}}}{\partial \mathbf{x}_{p}^{T}} &= \begin{bmatrix} \cos x_2\cos x_3 & -x_1\sin x_2\cos x_3 & -x_1\cos x_2\sin x_3 \\ \sin x_2 & x_1\cos x_2 & 0 \\ -\cos x_2\sin x_3 & x_1\sin x_2\sin x_3 & -x_1\cos x_2\cos x_3 \end{bmatrix}.
\end{aligned} \tag{24}$$

Equations (13) and (20) yield

$$\begin{aligned}
\mathbf{r}_{tc}^{\mathrm{B}} &= -\begin{bmatrix} x_{ct}^{\mathrm{I}}\left(q_0^2+q_1^2-q_2^2-q_3^2\right) + y_{ct}^{\mathrm{I}}\left(2q_1q_2+2q_0q_3\right) + z_{ct}^{\mathrm{I}}\left(2q_1q_3-2q_0q_2\right) \\ x_{ct}^{\mathrm{I}}\left(2q_1q_2-2q_0q_3\right) + y_{ct}^{\mathrm{I}}\left(q_0^2-q_1^2+q_2^2-q_3^2\right) + z_{ct}^{\mathrm{I}}\left(2q_0q_1+2q_2q_3\right) \\ x_{ct}^{\mathrm{I}}\left(2q_1q_3+2q_0q_2\right) + y_{ct}^{\mathrm{I}}\left(2q_2q_3-2q_0q_1\right) + z_{ct}^{\mathrm{I}}\left(q_0^2-q_1^2-q_2^2+q_3^2\right) \end{bmatrix},\\
\frac{\partial \mathbf{r}_{tc}^{\mathrm{B}}}{\partial \mathbf{q}^{T}} &= -[\mathbf{C}_1, \mathbf{C}_2],
\end{aligned} \tag{25}$$

where

$$\begin{aligned}
\mathbf{C}_1 &= \begin{bmatrix} 2q_0x_{ct}^{\mathrm{I}} + 2q_3y_{ct}^{\mathrm{I}} - 2q_2z_{ct}^{\mathrm{I}} & 2q_1x_{ct}^{\mathrm{I}} + 2q_2y_{ct}^{\mathrm{I}} + 2q_3z_{ct}^{\mathrm{I}} \\ -2q_3x_{ct}^{\mathrm{I}} + 2q_0y_{ct}^{\mathrm{I}} + 2q_1z_{ct}^{\mathrm{I}} & 2q_2x_{ct}^{\mathrm{I}} - 2q_1y_{ct}^{\mathrm{I}} + 2q_0z_{ct}^{\mathrm{I}} \\ 2q_2x_{ct}^{\mathrm{I}} - 2q_1y_{ct}^{\mathrm{I}} + 2q_0z_{ct}^{\mathrm{I}} & 2q_3x_{ct}^{\mathrm{I}} - 2q_0y_{ct}^{\mathrm{I}} - 2q_1z_{ct}^{\mathrm{I}} \end{bmatrix},\\
\mathbf{C}_2 &= \begin{bmatrix} -2q_2x_{ct}^{\mathrm{I}} + 2q_1y_{ct}^{\mathrm{I}} - 2q_0z_{ct}^{\mathrm{I}} & -2q_3x_{ct}^{\mathrm{I}} + 2q_0y_{ct}^{\mathrm{I}} + 2q_1z_{ct}^{\mathrm{I}} \\ 2q_1x_{ct}^{\mathrm{I}} + 2q_2y_{ct}^{\mathrm{I}} + 2q_3z_{ct}^{\mathrm{I}} & -2q_0x_{ct}^{\mathrm{I}} - 2q_3y_{ct}^{\mathrm{I}} + 2q_2z_{ct}^{\mathrm{I}} \\ 2q_0x_{ct}^{\mathrm{I}} + 2q_3y_{ct}^{\mathrm{I}} - 2q_2z_{ct}^{\mathrm{I}} & 2q_1x_{ct}^{\mathrm{I}} + 2q_2y_{ct}^{\mathrm{I}} + 2q_3z_{ct}^{\mathrm{I}} \end{bmatrix}.
\end{aligned} \tag{26}$$

3.3. Obstacle Potential Function. The obstacle is regarded as a sphere with a certain radius, and the expression of the obstacle potential function Ω_{o0} is

$$\Omega_{o0} = k_{1o}\exp\left(-\frac{1}{2k_{2o}^2}\left(\mathbf{r}_{oc}^{\mathrm{I}}\right)^{T}\cdot\mathbf{r}_{oc}^{\mathrm{I}}\right), \tag{27}$$

where $k_{1o} > 0$ represents the height of the potential function and $k_{2o} > 0$ can be considered as an approximate representation of the obstacle's radius. $\mathbf{r}_{oc}^{\mathrm{I}} = [x_{oc}^{\mathrm{I}}, y_{oc}^{\mathrm{I}}, z_{oc}^{\mathrm{I}}]$ is the position vector of the chaser relative to the spherical obstacle described in the frame $\mathscr{F}_{\mathrm{I}}$, and the expression of $\mathbf{r}_{oc}^{\mathrm{I}} \in \mathbb{R}^3$ is

$$\mathbf{r}_{oc}^{\mathrm{I}} = -\left(\left(\mathbf{M}_{\mathrm{I}}^{\mathrm{S}}\right)^{T}\cdot\mathbf{r}_{ct}^{\mathrm{S}} + \left(\mathbf{M}_{\mathrm{I}}^{\mathrm{B}}(\mathbf{q})\right)^{T}\cdot\mathbf{r}_{to}^{\mathrm{B}}\right), \tag{28}$$

where $\mathbf{r}_{ct}^{\mathrm{S}} = [r,0,0]^{T}$ is the position vector of the target relative to the chaser described in the frame $\mathscr{F}_{\mathrm{S}}$ and $\mathbf{r}_{to}^{\mathrm{B}} = [x_{to}^{\mathrm{B}}, y_{to}^{\mathrm{B}}, z_{to}^{\mathrm{B}}]$ is the position vector of the spherical obstacle relative to the target described in the frame $\mathscr{F}_{\mathrm{B}}$. When $\mathbf{r}_{to}^{\mathrm{B}} \in \mathbb{R}^3$ is unchanged, the obstacle remains hovering with the target. When $\mathbf{r}_{to}^{\mathrm{B}} \in \mathbb{R}^3$ changes, the obstacle is in relative motion with the target.

The time derivative of equation (27) gives

$$\begin{aligned}
\dot{\Omega}_{o0}\left(q, x_p, r_{to}^{\mathrm{B}}\right) &= \Omega_{o0}\left(\mathbf{q}, \mathbf{x}_p, \mathbf{r}_{to}^{\mathrm{B}}\right)\cdot\left(-\frac{1}{2k_{2o}^2}\right)\cdot 2\left(\mathbf{r}_{oc}^{\mathrm{I}}\right)^{T}\\
&\quad\cdot\left(\frac{\partial \mathbf{r}_{oc}^{\mathrm{I}}}{\partial \mathbf{x}_{p}^{T}}\frac{\partial \mathbf{x}_p}{\partial t} + \frac{\partial \mathbf{r}_{oc}^{\mathrm{I}}}{\partial \mathbf{q}^{T}}\frac{\partial \mathbf{q}}{\partial t} + \frac{\partial \mathbf{r}_{oc}^{\mathrm{I}}}{\partial\left(\left(\mathbf{r}_{to}^{\mathrm{B}}\right)^{T}\right)}\frac{\partial \mathbf{r}_{to}^{\mathrm{B}}}{\partial t}\right),
\end{aligned} \tag{29}$$

where

$$\frac{\partial \mathbf{r}_{oc}^{\mathrm{I}}}{\partial \mathbf{x}_p^T} = -\frac{\partial \mathbf{r}_{ct}}{\partial \mathbf{x}_p^T} = -\begin{bmatrix} \cos x_2 \cos x_3 & -x_1 \sin x_2 \cos x_3 & -x_1 \cos x_2 \sin x_3 \\ \sin x_2 & x_1 \cos x_2 & 0 \\ -\cos x_2 \sin x_3 & x_1 \sin x_2 \sin x_3 & -x_1 \cos x_2 \cos x_3 \end{bmatrix},$$
$$\frac{\partial \mathbf{r}_{oc}^{\mathrm{I}}}{\partial \left(\left(\mathbf{r}_{to}^{\mathrm{B}}\right)^T\right)} = \left(\mathbf{M}_{\mathrm{I}}^{\mathrm{B}}(\mathbf{q})\right)^T, \tag{30}$$
$$\frac{\partial \mathbf{r}_{to}^{\mathrm{B}}}{\partial t} = \left[\dot{x}_{to}^{\mathrm{B}}, \dot{y}_{to}^{\mathrm{B}}, \dot{z}_{to}^{\mathrm{B}}\right]^T.$$

Equation (13) and the expression of $\mathbf{r}_{to}^{\mathrm{B}} \in \mathbb{R}^3$ yield

$$\left(\mathbf{M}_{\mathrm{I}}^{\mathrm{B}}(\mathbf{q})\right)^T \cdot \mathbf{r}_{to}^{\mathrm{B}} = \begin{bmatrix} x_{to}^{\mathrm{B}}\left(q_0^2 + q_1^2 - q_2^2 - q_3^2\right) + y_{to}^{\mathrm{B}}\left(2q_1q_2 - 2q_0q_3\right) + z_{to}^{\mathrm{B}}\left(2q_1q_3 + 2q_0q_2\right) \\ x_{to}^{\mathrm{B}}\left(2q_1q_2 + 2q_0q_3\right) + y_{to}^{\mathrm{B}}\left(q_0^2 - q_1^2 + q_2^2 - q_3^2\right) + z_{to}^{\mathrm{B}}\left(2q_2q_3 - 2q_0q_1\right) \\ x_{to}^{\mathrm{B}}\left(2q_1q_3 - 2q_0q_2\right) + y_{to}^{\mathrm{B}}\left(2q_0q_1 + 2q_2q_3\right) + z_{to}^{\mathrm{B}}\left(q_0^2 - q_1^2 - q_2^2 + q_3^2\right) \end{bmatrix}, \tag{31}$$
$$\frac{\partial \mathbf{r}_{oc}^{\mathrm{I}}}{\partial \mathbf{q}^T} = [\mathbf{C}_3, \mathbf{C}_4],$$

where

$$\mathbf{C}_3 = \begin{bmatrix} 2q_0x_{to}^{\mathrm{B}} - 2q_3y_{to}^{\mathrm{B}} + 2q_2z_{to}^{\mathrm{B}} & 2q_1x_{to}^{\mathrm{B}} + 2q_2y_{to}^{\mathrm{B}} + 2q_3z_{to}^{\mathrm{B}} \\ 2q_3x_{to}^{\mathrm{B}} + 2q_0y_{to}^{\mathrm{B}} - 2q_1z_{to}^{\mathrm{B}} & 2q_2x_{to}^{\mathrm{B}} - 2q_1y_{to}^{\mathrm{B}} - 2q_0z_{to}^{\mathrm{B}} \\ -2q_2x_{to}^{\mathrm{B}} + 2q_1y_{to}^{\mathrm{B}} + 2q_0z_{to}^{\mathrm{B}} & 2q_3x_{to}^{\mathrm{B}} + 2q_0y_{to}^{\mathrm{B}} - 2q_1z_{to}^{\mathrm{B}} \end{bmatrix},$$
$$\mathbf{C}_4 = \begin{bmatrix} -2q_2x_{to}^{\mathrm{B}} + 2q_1y_{to}^{\mathrm{B}} + 2q_0z_{to}^{\mathrm{B}} & -2q_3x_{to}^{\mathrm{B}} - 2q_0y_{to}^{\mathrm{B}} + 2q_1z_{to}^{\mathrm{B}} \\ 2q_1x_{to}^{\mathrm{B}} + 2q_2y_{to}^{\mathrm{B}} + 2q_3z_{to}^{\mathrm{B}} & 2q_0x_{to}^{\mathrm{B}} - 2q_3y_{to}^{\mathrm{B}} + 2q_2z_{to}^{\mathrm{B}} \\ -2q_0x_{to}^{\mathrm{B}} + 2q_3y_{to}^{\mathrm{B}} - 2q_2z_{to}^{\mathrm{B}} & 2q_1x_{to}^{\mathrm{B}} + 2q_2y_{to}^{\mathrm{B}} + 2q_3z_{to}^{\mathrm{B}} \end{bmatrix}. \tag{32}$$

3.4. Total Potential Function. The total potential function Ω_0 is the sum of the attractive potential function Ω_d, the safe potential function Ω_{s0}, and the obstacle potential function Ω_{o0}, and the expression of Ω_0 is

$$\begin{aligned} \Omega_0 &= \Omega_d + \Omega_{s0} + \Omega_{o0} \\ &= \frac{1}{2}\mathbf{e}_p^T\mathbf{Q}_p\mathbf{e}_p + \frac{1}{2}\mathbf{e}_v^T\mathbf{Q}_v\mathbf{e}_v + k_{1s}\exp\left(-\frac{1}{2k_{2s}^2}\left|f\left(\mathbf{r}_{tc}^{\mathrm{B}}\right)\right|\right) \\ &\quad + k_{1o}\exp\left(-\frac{1}{2k_{2o}^2}\left(\mathbf{r}_{oc}^{\mathrm{I}}\right)^T \cdot \mathbf{r}_{oc}^{\mathrm{I}}\right). \end{aligned} \tag{33}$$

It can be concluded from equation (33) that the minimum value of Ω_0 is no longer precisely located in the reference position state. To avoid the above situation, the safe potential function Ω_{s0} of equation (19) and the obstacle potential function Ω_{o0} of equation (27) are redefined, each adding a quadratic term, which yields

$$\Omega_s = \frac{1}{2}\mathbf{e}_p^T\mathbf{Q}_s\mathbf{e}_pk_{1s}\exp\left(-\frac{1}{2k_{2s}^2}\left|f\left(\mathbf{r}_{tc}^{\mathrm{B}}\right)\right|\right), \tag{34}$$

$$\Omega_o = \frac{1}{2}\mathbf{e}_p^T\mathbf{Q}_o\mathbf{e}_pk_{1o}\exp\left(-\frac{1}{2k_{2o}^2}\left(\mathbf{r}_{oc}^{\mathrm{I}}\right)^T \cdot \mathbf{r}_{oc}^{\mathrm{I}}\right), \tag{35}$$

where $\mathbf{Q}_s \in \mathbb{R}^{3\times3}$ and $\mathbf{Q}_o \in \mathbb{R}^{3\times3}$ are positive definite symmetric matrices. Then, the modified system total potential function Ω expression is

$$\begin{aligned} \Omega &= \Omega_d + \Omega_s + \Omega_o \\ &= \frac{1}{2}\mathbf{e}_p^T\mathbf{Q}_p\mathbf{e}_p + \frac{1}{2}\mathbf{e}_v^T\mathbf{Q}_v\mathbf{e}_v + \frac{1}{2}\mathbf{e}_p^T\mathbf{Q}_s\mathbf{e}_pk_{1s}\exp\left(-\frac{1}{2k_{2s}^2}\left|f\left(\mathbf{r}_{tc}^{\mathrm{B}}\right)\right|\right) \\ &\quad + \frac{1}{2}\mathbf{e}_p^T\mathbf{Q}_o\mathbf{e}_pk_{1o}\exp\left(-\frac{1}{2k_{2o}^2}\left(\mathbf{r}_{oc}^{\mathrm{I}}\right)^T \cdot \mathbf{r}_{oc}^{\mathrm{I}}\right). \end{aligned} \tag{36}$$

As can be seen from equation (36), the total potential function Ω has a global minimum at the reference position ($\mathbf{e}_p = 0$ and $\mathbf{e}_v = 0$). It should be pointed out that, in order to facilitate the analysis, equation (36) only considers the case of single obstacle. When there are multiple obstacles, it only needs to change Ω_o in equation (35) to $\sum_i \Omega_{oi}$.

4. Proof of System Stability

Proof. The modified total potential function Ω is taken as Lyapunov function V, i.e.,

$$V = \frac{1}{2}\mathbf{e}_p^T\mathbf{Q}_p\mathbf{e}_p + \frac{1}{2}\mathbf{e}_v^T\mathbf{Q}_v\mathbf{e}_v + \frac{1}{2}\mathbf{e}_p^T\mathbf{Q}_s\mathbf{e}_p k_{1s}\exp\left(-\frac{1}{2k_{2s}^2}\left|f\left(\mathbf{r}_{tc}^{\mathrm{B}}\right)\right|\right) + \frac{1}{2}\mathbf{e}_p^T\mathbf{Q}_o\mathbf{e}_p k_{1o}\exp\left(-\frac{1}{2k_{2o}^2}\left(\mathbf{r}_{oc}^{\mathrm{I}}\right)^T\cdot\mathbf{r}_{oc}^{\mathrm{I}}\right). \tag{37}$$

As can be obtained from equation (37), $V \geq 0$. $V = 0$ only when $\mathbf{e}_p = [0,0,0]^T$ and $\mathbf{e}_v = [0,0,0]^T$, otherwise $V > 0$. When $\mathbf{e}_p = [0,0,0]^T$ and $\mathbf{e}_v = [0,0,0]^T$, the chaser has reached the desired position. The time derivative of equation (37) gives

$$\begin{aligned}\dot{V} &= \mathbf{e}_p^T\mathbf{Q}_p\dot{\mathbf{e}}_p + \mathbf{e}_v^T\mathbf{Q}_v\dot{\mathbf{e}}_v + \mathbf{e}_p^T\mathbf{Q}_s\dot{\mathbf{e}}_p\cdot\Omega_{s0}\left(\mathbf{q},\mathbf{x}_p\right) \\ &\quad + \frac{1}{2}\mathbf{e}_p^T\mathbf{Q}_s\mathbf{e}_p\cdot\dot{\Omega}_{s0}\left(\mathbf{q},\mathbf{x}_p\right) + \mathbf{e}_p^T\mathbf{Q}_o\dot{\mathbf{e}}_p\cdot\Omega_{o0}\left(\mathbf{q},\mathbf{x}_p,\mathbf{r}_{to}^{\mathrm{B}}\right) \\ &\quad + \frac{1}{2}\mathbf{e}_p^T\mathbf{Q}_o\mathbf{e}_p\cdot\dot{\Omega}_{o0}\left(\mathbf{q},\mathbf{x}_p,\mathbf{r}_{to}^{\mathrm{B}}\right).\end{aligned} \tag{38}$$

Substituting equations (7) and (8) into equation (38) yields

$$\begin{aligned}\dot{V} &= \mathbf{e}_p^T\mathbf{Q}_p\dot{\mathbf{e}}_p + \left(\mathbf{P}_1^{-1}(x)\dot{\mathbf{e}}_p\right)^T\mathbf{Q}_v\left(\dot{\mathbf{x}}_v - \mathbf{P}_2(x)\right) \\ &\quad + \mathbf{e}_p^T\mathbf{Q}_s\dot{\mathbf{e}}_p\cdot\Omega_{s0}\left(\mathbf{q},\mathbf{x}_p\right) + \frac{1}{2}\mathbf{e}_p^T\mathbf{Q}_s\mathbf{e}_p\cdot\dot{\Omega}_{s0}\left(\mathbf{q},\mathbf{x}_p\right) \\ &\quad + \mathbf{e}_p^T\mathbf{Q}_o\dot{\mathbf{e}}_p\cdot\Omega_{o0}\left(\mathbf{q},\mathbf{x}_p,\mathbf{r}_{to}^{\mathrm{B}}\right) + \frac{1}{2}\mathbf{e}_p^T\mathbf{Q}_o\mathbf{e}_p\cdot\dot{\Omega}_{o0}\left(\mathbf{q},\mathbf{x}_p,\mathbf{r}_{to}^{\mathrm{B}}\right) \\ &= \mathbf{e}_p^T\mathbf{Q}_p\dot{\mathbf{e}}_p + \dot{\mathbf{e}}_p^T\mathbf{P}_1^{-1}(x)\mathbf{Q}_v\left(\dot{\mathbf{x}}_v - \mathbf{P}_2(x)\right) \\ &\quad + \mathbf{e}_p^T\mathbf{Q}_s\dot{\mathbf{e}}_p\cdot\Omega_{s0}\left(\mathbf{q},\mathbf{x}_p\right) + \frac{1}{2}\mathbf{e}_p^T\mathbf{Q}_s\mathbf{e}_p\cdot\dot{\Omega}_{s0}\left(\mathbf{q},\mathbf{x}_p\right) \\ &\quad + \mathbf{e}_p^T\mathbf{Q}_o\dot{\mathbf{e}}_p\cdot\Omega_{o0}\left(\mathbf{q},\mathbf{x}_p,\mathbf{r}_{to}^{\mathrm{B}}\right) + \frac{1}{2}\mathbf{e}_p^T\mathbf{Q}_o\mathbf{e}_p\cdot\dot{\Omega}_{o0}\left(\mathbf{q},\mathbf{x}_p,\mathbf{r}_{to}^{\mathrm{B}}\right),\end{aligned} \tag{39}$$

Let

$$\begin{aligned}\mathbf{P}_1^{-1}(x)\mathbf{Q}_v\left(\dot{\mathbf{x}}_v - \mathbf{P}_2(x)\right) &= -\mathbf{Q}_p\mathbf{e}_p - \mathbf{Q}_l\dot{\mathbf{e}}_p - \mathbf{Q}_s\mathbf{e}_p\cdot\Omega_{s0}\left(\mathbf{q},\mathbf{x}_p\right) \\ &\quad - \frac{1}{2}\mathbf{Q}_n\mathbf{e}_p^T\mathbf{Q}_s\mathbf{e}_p\cdot\dot{\Omega}_{s0}\left(\mathbf{q},\mathbf{x}_p\right) \\ &\quad - \mathbf{Q}_o\mathbf{e}_p\cdot\Omega_{o0}\left(\mathbf{q},\mathbf{x}_p,\mathbf{r}_{to}^{\mathrm{B}}\right) \\ &\quad - \frac{1}{2}\mathbf{Q}_n\mathbf{e}_p^T\mathbf{Q}_o\mathbf{e}_p\cdot\dot{\Omega}_{s0}\left(\mathbf{q},\mathbf{x}_p,\mathbf{r}_{to}^{\mathrm{B}}\right),\end{aligned} \tag{40}$$

where $\mathbf{Q}_l \in \mathbb{R}^{3\times3}$ is positive definite symmetric matrix. $\mathbf{Q}_n \in \mathbb{R}^{3\times3}$ is the generalized inverse matrix of $\dot{e}_p^T$, and the expression of $\mathbf{Q}_n \in \mathbb{R}^{3\times3}$ is

$$\mathbf{Q}_n = \left(\dot{\mathbf{e}}_P\dot{\mathbf{e}}_p^T\right)^{-1}\dot{\mathbf{e}}_P. \tag{41}$$

Equation (40) yields

$$\begin{aligned}\dot{x}_v &= \mathbf{Q}_v^{-1}\mathbf{P}_1(x)\Big(-\mathbf{Q}_p\mathbf{e}_p - \mathbf{Q}_l\dot{\mathbf{e}}_p - \mathbf{Q}_s\mathbf{e}_p\cdot\Omega_{s0}\left(\mathbf{q},\mathbf{x}_p\right) \\ &\quad - \frac{1}{2}\mathbf{Q}_n\mathbf{e}_p^T\mathbf{Q}_s\mathbf{e}_p\cdot\dot{\Omega}_{s0}\left(\mathbf{q},\mathbf{x}_p\right) - \mathbf{Q}_o\mathbf{e}_p\cdot\Omega_{o0}\left(\mathbf{q},\mathbf{x}_p,\mathbf{r}_{to}^{\mathrm{B}}\right) \\ &\quad - \frac{1}{2}\mathbf{Q}_n\mathbf{e}_p^T\mathbf{Q}_o\mathbf{e}_p\cdot\dot{\Omega}_{s0}\left(\mathbf{q},\mathbf{x}_p,\mathbf{r}_{to}^{\mathrm{B}}\right)\Big) + \mathbf{P}_2(x) \\ &= \mathbf{P}_2(x) - \mathbf{Q}_v^{-1}\mathbf{P}_1(x)\left(\mathbf{Q}_p\mathbf{e}_p + \mathbf{Q}_l\mathbf{P}_1(x)\mathbf{e}_v\right) \\ &\quad + \mathbf{Q}_v^{-1}\mathbf{P}_1(x)\Big(-\mathbf{Q}_s\mathbf{e}_p\cdot\Omega_{s0}\left(\mathbf{q},\mathbf{x}_p\right) \\ &\quad - \frac{1}{2}\mathbf{Q}_n\mathbf{e}_p^T\mathbf{Q}_s\mathbf{e}_p\cdot\dot{\Omega}_{s0}\left(\mathbf{q},\mathbf{x}_p\right)\Big) \\ &\quad + \mathbf{Q}_v^{-1}\mathbf{P}_1(x)\Big(-\mathbf{Q}_o\mathbf{e}_p\cdot\Omega_{o0}\left(\mathbf{q},\mathbf{x}_p,\mathbf{r}_{to}^{\mathrm{B}}\right) \\ &\quad - \frac{1}{2}\mathbf{Q}_n\mathbf{e}_p^T\mathbf{Q}_o\mathbf{e}_p\cdot\dot{\Omega}_{s0}\left(\mathbf{q},\mathbf{x}_p,\mathbf{r}_{to}^{\mathrm{B}}\right)\Big) \\ &= \mathbf{a}_t + \mathbf{a}_s + \mathbf{a}_o,\end{aligned} \tag{42}$$

where

$$\begin{aligned}\mathbf{a}_t &= \mathbf{P}_2(x) - \mathbf{Q}_v^{-1}\mathbf{P}_1(x)\left(\mathbf{Q}_p\mathbf{e}_p + \mathbf{Q}_l\mathbf{P}_1(x)\mathbf{e}_v\right), \\ \mathbf{a}_s &= -\mathbf{Q}_v^{-1}\mathbf{P}_1(x)\Big(\mathbf{Q}_s\mathbf{e}_p\cdot\Omega_{s0}\left(\mathbf{q},\mathbf{x}_p\right) \\ &\quad + \frac{1}{2}\mathbf{Q}_n\mathbf{e}_p^T\mathbf{Q}_s\mathbf{e}_p\cdot\dot{\Omega}_{s0}\left(\mathbf{q},\mathbf{x}_p\right)\Big), \\ \mathbf{a}_o &= -\mathbf{Q}_v^{-1}\mathbf{P}_1(x)\Big(\mathbf{Q}_o\mathbf{e}_p\cdot\Omega_{o0}\left(\mathbf{q},\mathbf{x}_p,\mathbf{r}_{to}^{\mathrm{B}}\right) \\ &\quad + \frac{1}{2}\mathbf{Q}_n\mathbf{e}_p^T\mathbf{Q}_o\mathbf{e}_p\cdot\dot{\Omega}_{s0}\left(\mathbf{q},\mathbf{x}_p,\mathbf{r}_{to}^{\mathrm{B}}\right)\Big),\end{aligned} \tag{43}$$

where $\mathbf{a}_t \in \mathbb{R}^3$ represents the gravitational acceleration of the reference position potential field to the chaser, $\mathbf{a}_s \in \mathbb{R}^3$ represents the repulsive acceleration of the safe corridor potential field to the chaser, and $\mathbf{a}_o \in \mathbb{R}^3$ represents the repulsive acceleration of the obstacle potential field to the chaser. Substituting equation (40) into (39) yields

$$\dot{V} = -\dot{\mathbf{e}}_p^T\mathbf{Q}_l\dot{\mathbf{e}}_p \leq 0. \tag{44}$$

This case completes the proof.

The control acceleration vector of the system in the frame $\mathcal{F}_S$ is derived from equations (46) and (3):

$$\mathbf{a} = \operatorname{diag}(-1,-1,1)\dot{\mathbf{x}}_v + \begin{bmatrix} \dfrac{\left(x_5^2 + x_6^2\right)}{x_1} \\ \dfrac{-x_4 x_5}{x_1} - \dfrac{x_6^2 \sin x_2}{\left(x_1 \cos x_2\right)} \\ \dfrac{x_4 x_6}{x_1} - \dfrac{x_5 x_6 \sin x_2}{\left(x_1 \cos x_2\right)} \end{bmatrix}. \tag{45}$$

Due to the limited thrust of the chaser, its control acceleration is limited, and the actual control acceleration in each direction is

$$a_c = \begin{cases} a_{\max}, & a > a_{\max}, \\ a, & -a_{\max} \le a \le a_{\max}, \\ -a_{\max}, & a < -a_{\max}, \end{cases} \tag{46}$$

where $a_{\max} \in \mathbb{R}$ is the maximum acceleration that can be provided by the chaser in a single direction and $a \in \mathbb{R}$ is the acceleration obtained by using equation (46). □

5. Simulation Example

In this paper, the numerical simulation of the autonomous rendezvous and docking mission of the chaser spacecraft relative to the noncooperative target spacecraft in super close range is carried out. In order to visually analyze the effect of attractive potential function, safe potential function, and obstacle potential function, three sets of simulation scenarios are set up in this paper:

(1) The action of the attractive potential function alone is considered

(2) The actions of both the attractive potential function and safe potential function are considered

(3) The actions of all he attractive potential function, safe potential function, and obstacle potential function are considered

It is assumed that the target spacecraft is in free-tumbling state without external torque in space, and there is no maneuver in the target. The initial states of the target and chaser in the frame $\mathscr{F}_{\mathrm{I}}$ are

$$\begin{aligned} \mathbf{r}_t^{\mathrm{I}}(t_0) &= [-1535849.23, 5181325.49, 4056754.35]^T \text{ m}, \\ \mathbf{v}_t^{\mathrm{I}}(t_0) &= [-4902.795, -4476.845, 3880.881]^T \text{ m/s}, \\ \mathbf{r}_c^{\mathrm{I}}(t_0) &= [-1535824.62, 5181205.19, 4056813.08]^T \text{ m}, \\ \mathbf{v}_c^{\mathrm{I}}(t_0) &= [-4902.895, -4476.765, 3880.981]^T \text{ m}. \end{aligned} \tag{47}$$

The docking position in the frame $\mathscr{F}_{\mathrm{B}}$ is $\mathbf{r}_d^{\mathrm{B}} = [5, 0, 0]^T$ m. The initial attitude quaternion and angular velocity of the target are $\mathbf{q}_t(t_0) = [-0.0094, -0.5443, 0.2292, -0.8069]^T$ and $\boldsymbol{\omega}_c(t_0) = [-0.0035, 0.0052, 0.0035]^T$ rad/s. The maximum control acceleration in each direction provided by the chaser is $a_{\max} = 0.2\text{m/s}^2$. The parameters of the attractive potential function are $\mathbf{Q}_v = \operatorname{diag}(1,1,1)$, $\mathbf{Q}_p = \operatorname{diag}(100,100,100)$, and $\mathbf{Q}_v = \operatorname{diag}(2500,2500,2500)$. The parameters of the safe potential function are $\mathbf{Q}_s = \operatorname{diag}(0.001, 0.001, 0.001)$, $k_{1s} = 10^5$, and $k_{2s} = 25$. The parameters of the obstacle potential function are $\mathbf{Q}_o = \operatorname{diag}(0.001, 0.001, 0.001)$, $k_{1o} = 10^6$, and $k_{2o} = 6$. The parameters of the elliptical vine curve function are $\rho = 20$ and $\varphi = 10^\circ$. The safe distance of the target's safe corridor is $\rho_s = 20$ m, and the safe angle is $\varphi_s = 10^\circ$. The moment of inertia of the target is

$$\mathbf{J}_t = \begin{bmatrix} 3336.3 & -135.4 & -154.2 \\ -135.4 & 3184.5 & -148.5 \\ -154.2 & -148.5 & 2423.7 \end{bmatrix} \text{kg}\cdot\text{m}^2 \tag{48}$$

The simulation time is 200 s, and the simulation step is 0.05 s.

Scenario 1. The action of the attractive potential function alone is considered. $\mathbf{Q}_s$ and $\mathbf{Q}_o$ in equation (42) are set as $\mathbf{Q}_s = \operatorname{diag}(0,0,0)$ and $\mathbf{Q}_o = \operatorname{diag}(0,0,0)$, respectively. The simulation results are presented in Figures 4–10.

Figure 4 shows the attitude and angular velocity of the target spacecraft, and the attitude and angular velocity of the target vary with time. Figure 5 shows the relative position and relative velocity of the chaser and the desired position. Figure 6 shows the errors of states. After 146 s, the chaser reaches the desired position, and the relative velocity of the chaser to the desired position is 0 m/s, after which the relative position and relative velocity of the chaser to the desired position remain unchanged.

Figure 7 shows the relative motion of the chaser and target in the frame $\mathscr{F}_{\mathrm{B}}$. Figure 8 shows the safe profile. From Figures 7 and 8, it can be conclude that the chaser crosses the safe corridor during the autonomous rendezvous and docking, and the chaser may collide with the accessories of the noncooperative target.

Figure 9 shows the control acceleration in the frame $\mathscr{F}_{\mathrm{S}}$. In order to keep up with the desired position, the chaser's line-of-sight direction (x-direction) always needs to provide a control acceleration, which changes back and forth between -0.2 m/s^2 and 0.2 m/s^2. The control acceleration in the y direction and the z direction changes dramatically at the initial time. After 81 s, the control acceleration in the y direction and the z direction maintained at an extremely small value of less than 0.002 m/s^2.

Scenario 1 shows that when the safe requirements are not considered, the autonomous rendezvous and docking with the noncooperative target by the chaser can be realized by the guidance of the attractive potential function. When considering the safe requirements, it is obvious that the attractive potential function alone cannot satisfy the requirements of safe rendezvous and docking.

Scenario 2. The action of the attractive potential function and safe potential function are both considered, and the other simulation conditions are the same as scenario 1. $\mathbf{Q}_o$ in

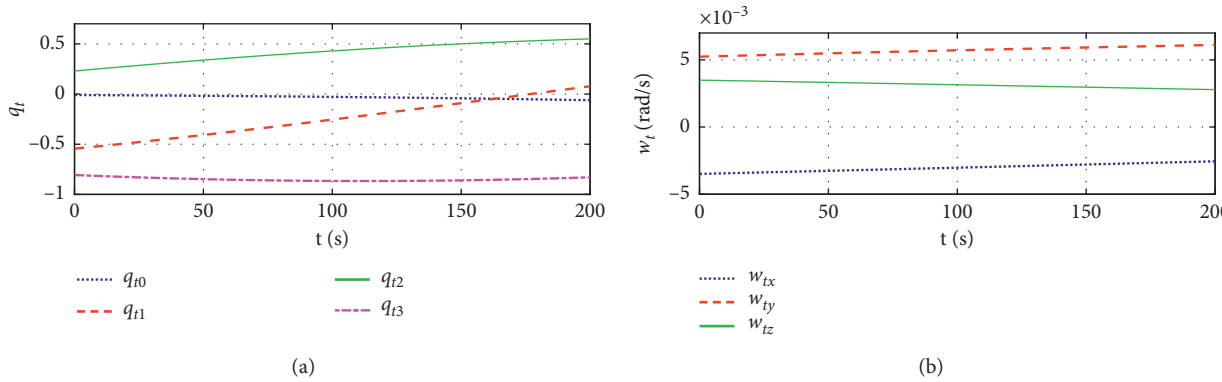

Figure 5: (a) Attitude and (b) angular velocity of the target.

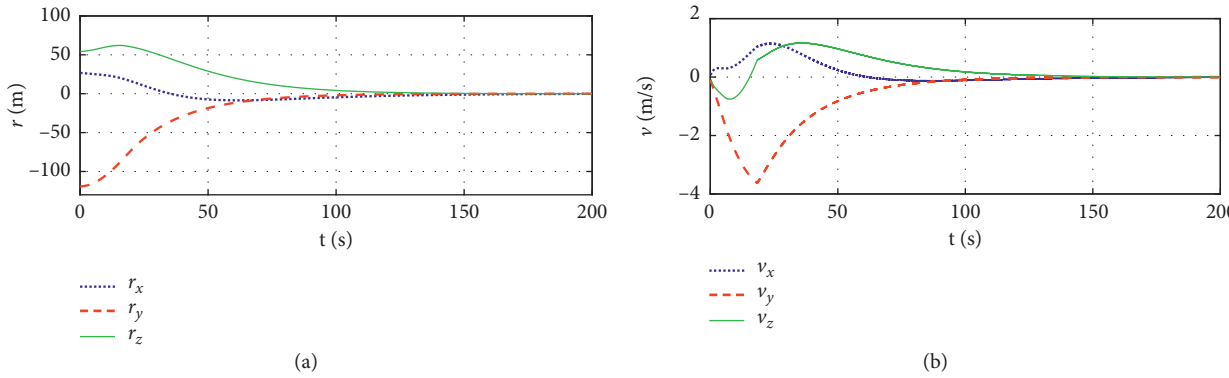

Figure 5: (a) Relative position and (b) relative velocity of the chaser and the desired position (Scenario 1).

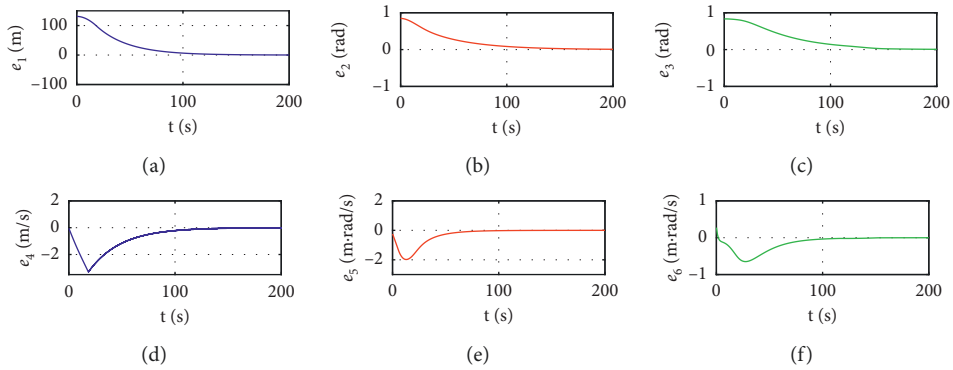

Figure 6: Errors of states (Scenario 1).

equation (42) is set as $\mathbf{Q}_o = \text{diag}(0, 0, 0)$. The simulation results are presented in Figures 10–14.

It can be concluded from Figure 10 that the relative position of the chaser and the desired position is 0 m after 103 s, and the relative velocity is 0 m/s. Figures 12 and 13 indicate that when considering the safe potential function, the chaser first approaches the target's docking direction, and then slowly approaches the target along the docking direction without colliding with the safe corridor. Figure 14 shows that, after 69 s, the control acceleration in the y direction and z direction tends to 0 m/s^2, and the control acceleration in the x direction changes back and forth between -0.2 m/s^2 and 0.2 m/s^2. Scenario 2 indicates that when considering the action of the safe potential function, the APF guidance can realize rendezvous and docking with noncooperative targets along the safe corridor. During the rendezvous and docking process, collision with the accessories of the target can be avoided, and the safe requirements can be guaranteed.

Scenario 3. Adding an obstacle to the path of autonomous rendezvous and docking in Scenario 2, the action of the attractive potential function, safe potential function, and

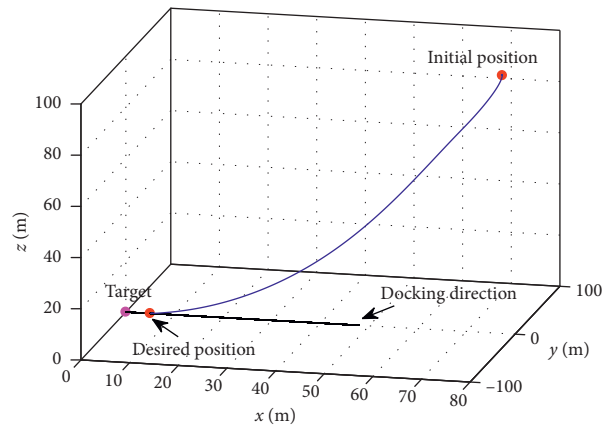

Figure 7: Relative motion of the chaser and target in the frame $\mathcal{F}_B$ (Scenario 1).

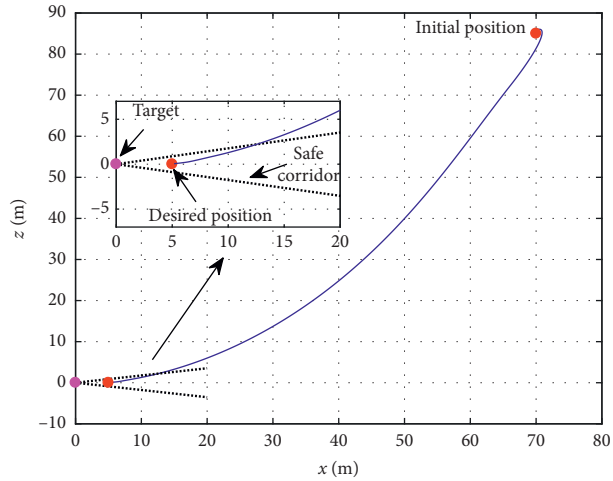

Figure 8: Safe profile (Scenario 1).

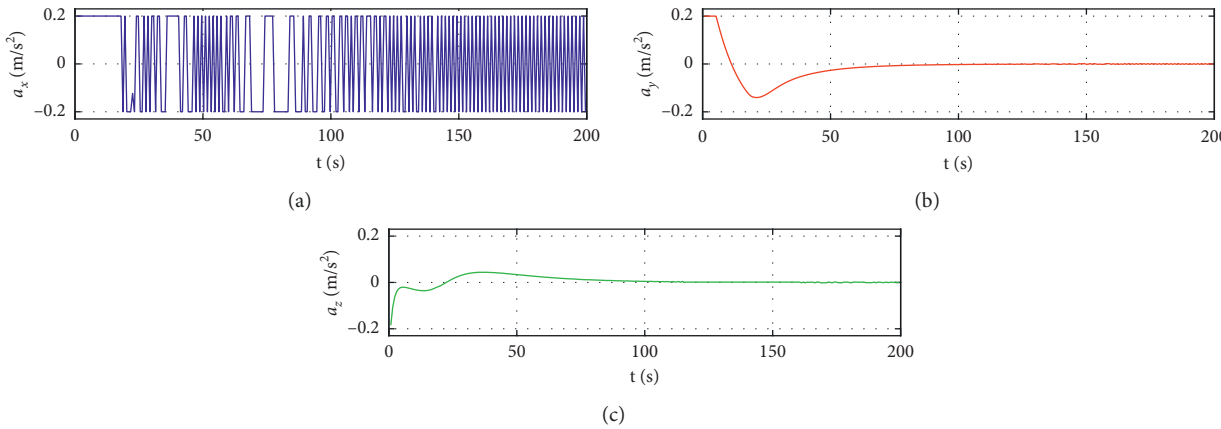

Figure 9: Control acceleration in the frame $\mathcal{F}_S$ (Scenario 1).

obstacle potential function are all considered. The simulation results are presented in Figures 15–19.

Figure 15 shows that the chaser has reached the desired position, the relative position is reduced to 0, and the relative speed is reduced to $\mathbf{0}$ m/s^2. Figures 17 and 18 indicate that the chaser can effectively avoid obstacle and achieve safe rendezvous and docking with noncooperative target when considering the action of the obstacle potential function. Figure 19 shows that, after a period of time, the control

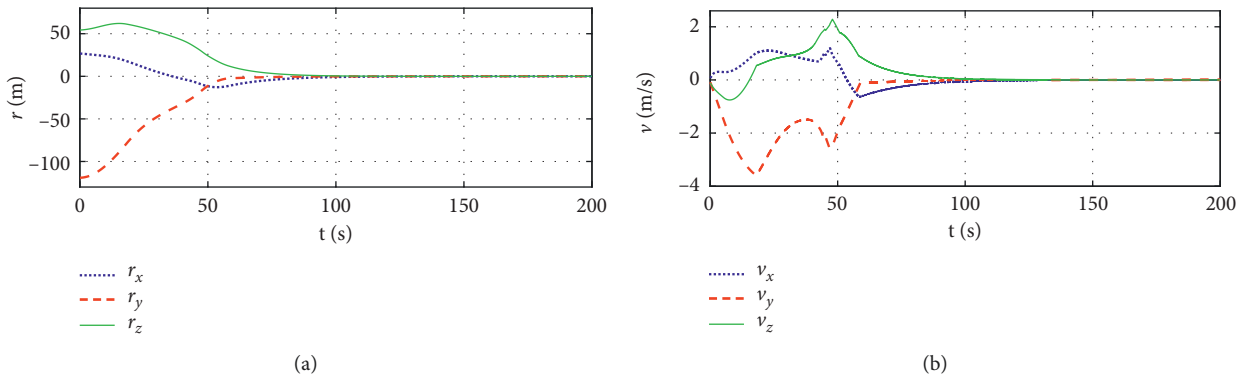

Figure 10: (a) Relative position and (b) relative velocity of the chaser and the desired position (Scenario 2).

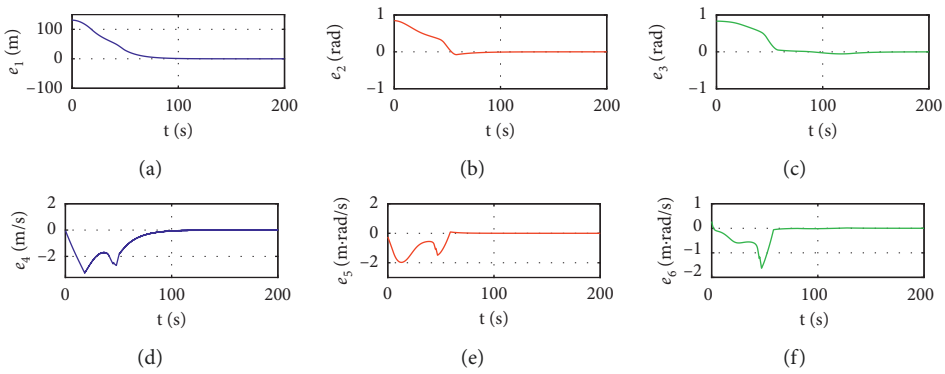

Figure 11: Errors of states (Scenario 2).

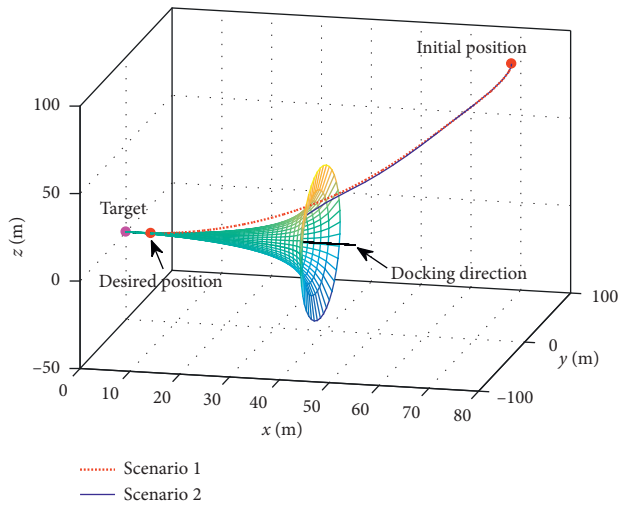

Figure 12: Relative motion of the chaser and target in the frame $\mathcal{F}_B$ (Scenario 2).

acceleration in the y direction and z direction tends to $0\,m/s^2$, and the control acceleration in the x direction changes back and forth between $-0.2\,m/s^2$ and $0.2\,m/s^2$.

Scenario 3 indicates that when considering the action of the obstacle potential function, the APF guidance can ensure the chaser effectively avoids the obstacles. The chaser approaches the noncooperative target along the safe corridor, which ensures the guidance requirements of safe rendezvous and docking and obstacle avoidance.

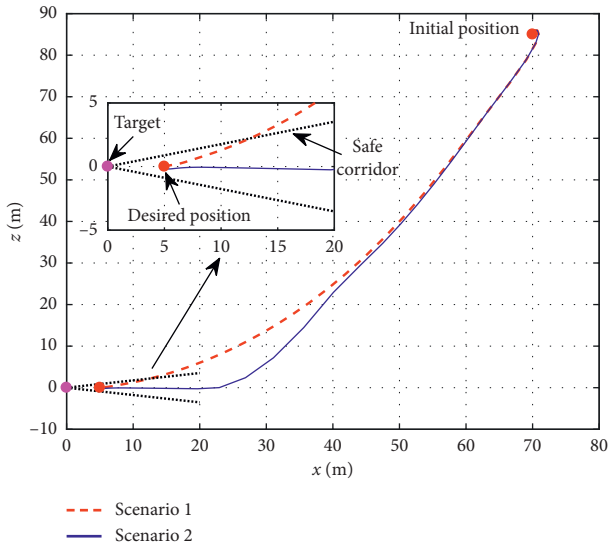

Figure 13: Safe profile (Scenario 2).

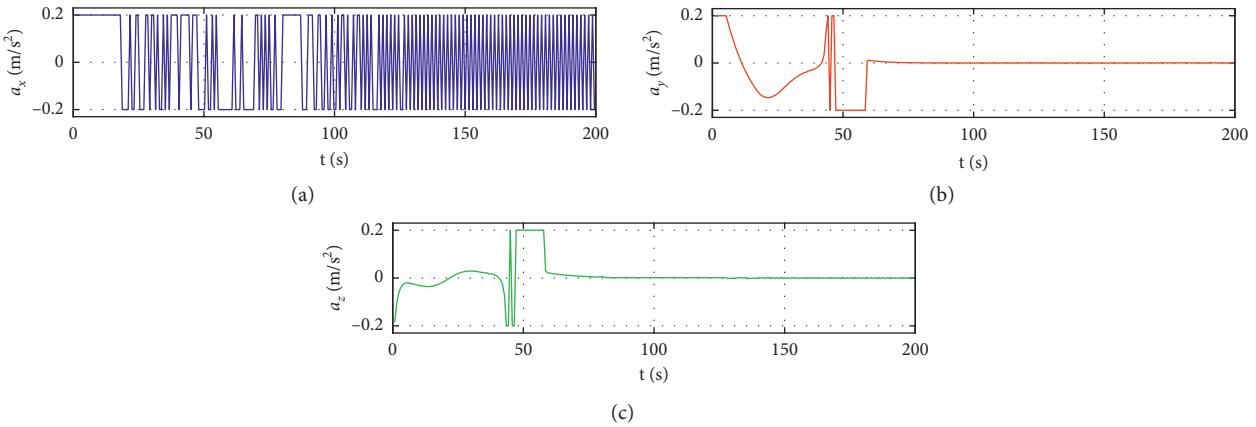

Figure 14: Control acceleration in the frame $\mathcal{F}_S$ (Scenario 2).

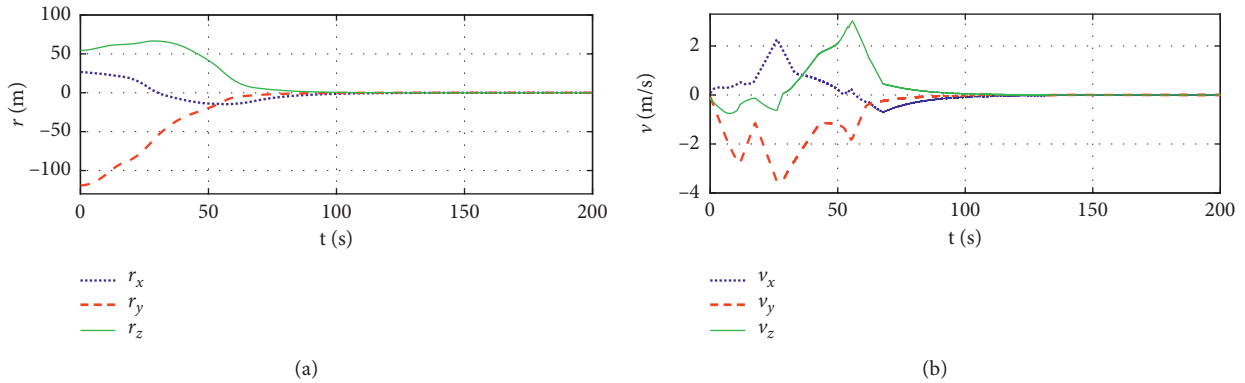

Figure 15: Relative position and relative velocity of the chaser and the desired position (Scenario 3).

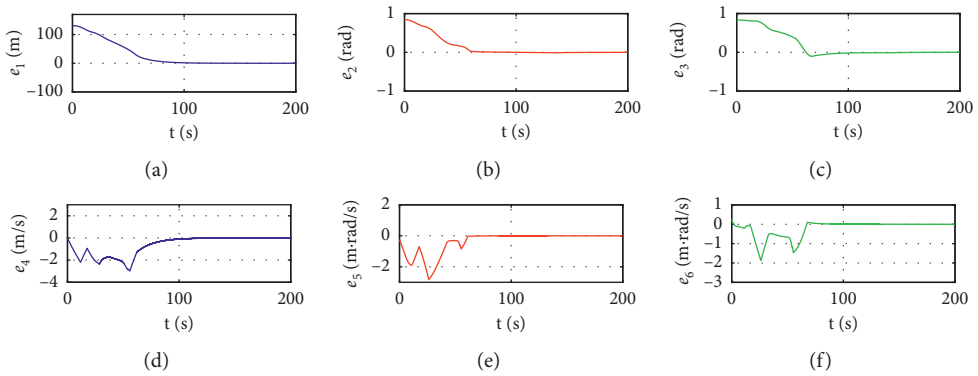

Figure 16: Errors of states (Scenario 3).

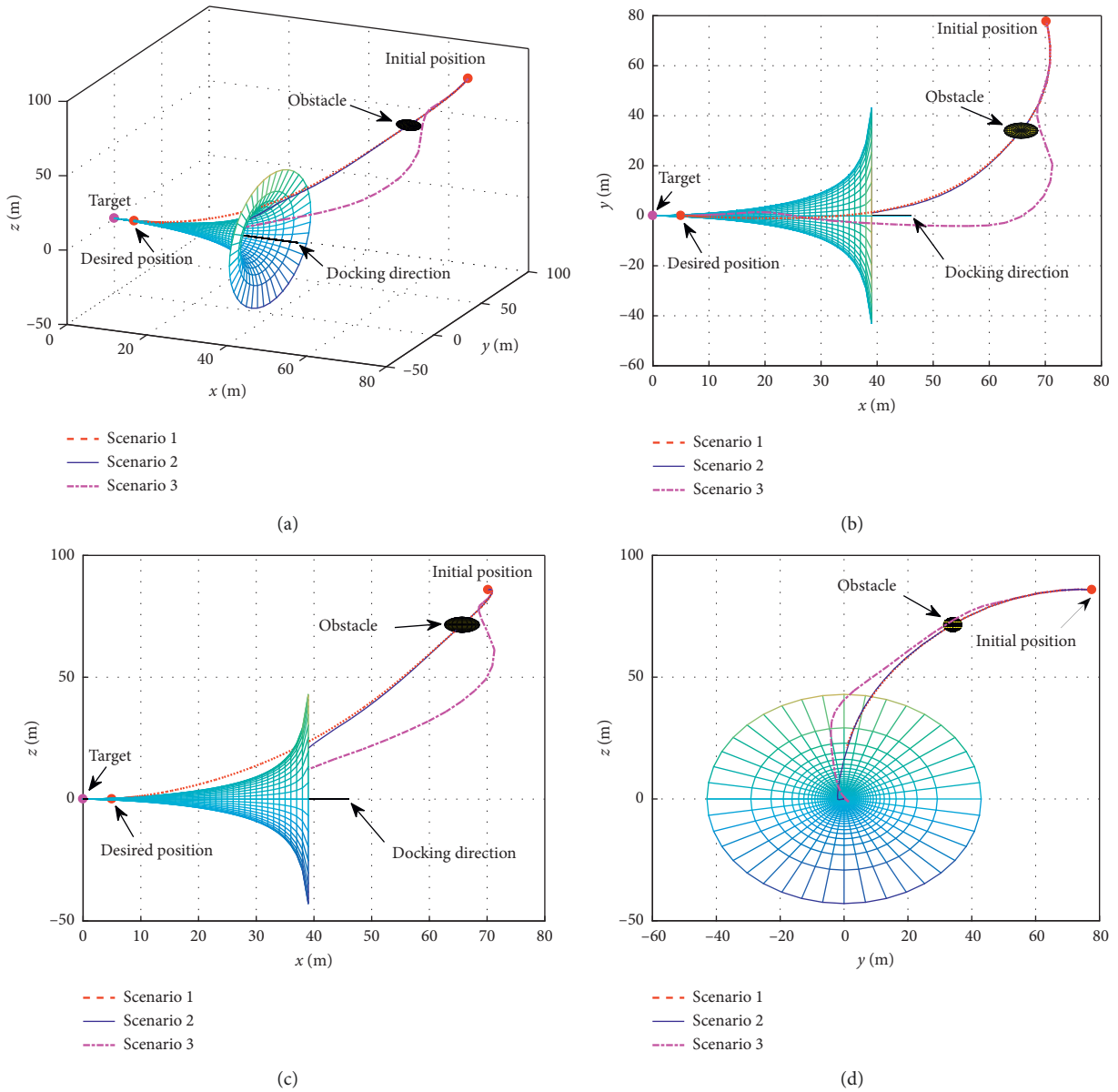

Figure 17: Relative motion of the chaser and target in the frame $\mathcal{F}_B$ (Scenario 3).

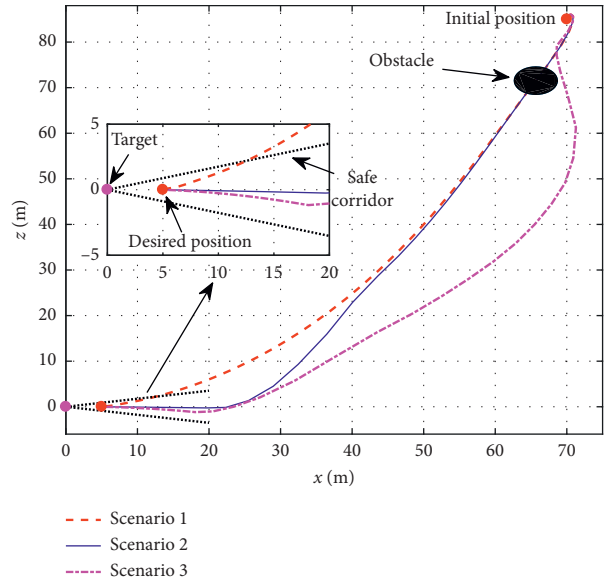

Figure 18: Safe profile (Scenario 3).

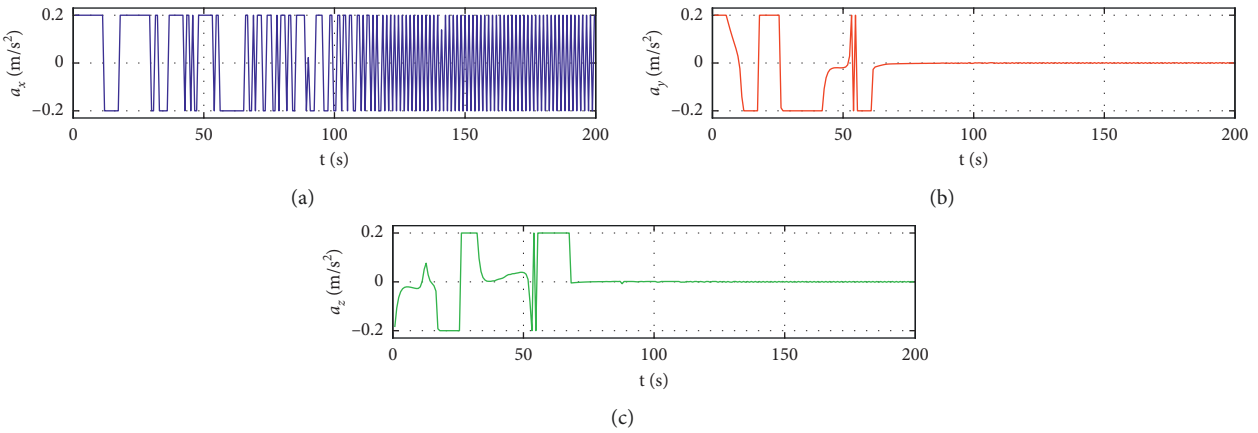

Figure 19: Control acceleration in the frame $\mathcal{F}_S$ (Scenario 3).

6. Conclusions

The problem of the APF safe approach and obstacle avoidance for autonomous rendezvous and docking of chaser to noncooperative target spacecraft is studied. The relative motion equation of the chaser relative to the noncooperative target spacecraft is established, and the attitude motion characteristics of the target spacecraft are analyzed. The attractive potential function, safe potential function, and obstacle potential function are designed. The time derivatives of the safe potential function and the obstacle potential function are obtained, respectively. The total potential function of the system is derived and modified. The stability of the system is analyzed according to Lyapunov theory, and the control acceleration of the chaser is derived. Finally, the numerical simulation is carried out, and the conclusions are as follows:

(1) The autonomous rendezvous and docking with the noncooperative target by the chaser can be realized by the guidance of the attractive potential function. When considering the safe requirements, it is obvious that the attractive potential function alone cannot satisfy the requirements of safe rendezvous and docking.

(2) When considering the action of the safe potential function, the APF guidance can realize rendezvous and docking with noncooperative targets along the safe corridor. During the rendezvous and docking process, collision with the accessories of the target can be avoided, and the safety requirements can be guaranteed.

(3) When considering the action of the obstacle potential function, the APF guidance can ensure the

chaser effectively avoids the obstacles. The chaser approaches the noncooperative target along the safe corridor, which ensures the guidance requirements of safe rendezvous and docking and obstacle avoidance.

Data Availability

The data used to support the findings of this study are included within the article.

Conflicts of Interest

The authors declare that they have no conflicts of interests.

Acknowledgments

The authors are grateful to Prof. Li and Scholar Hao for discussions. This paper was supported by the National Natural Science Foundation of China (no. 11472301).

References

[1] S. Bandyopadhyay, S.-J. Chung, and F. Y. Hadaegh, "Nonlinear attitude control of spacecraft with a large captured object," *Journal of Guidance, Control, and Dynamics*, vol. 39, no. 4, pp. 1–16, 2016.

[2] L. Zhang, S. Qian, S. Zhang, and H. Cai, "Research on angles-only/SINS/CNS relative position and attitude determination algorithm for a tumbling spacecraft," *Proceedings of the Institution of Mechanical Engineers, Part G: Journal of Aerospace Engineering*, vol. 231, no. 2, pp. 218–228, 2017.

[3] Y. She, J. Sun, S. Li, and T. Song, "Quasi-model free control for the post-capture operation of a non-cooperative target," *Acta Astronautica*, vol. 147, pp. 50–70, 2018.

[4] G. Zhao, S. Xu, and Y. Bo, "LiDAR-based non-cooperative tumbling spacecraft pose tracking by fusing depth maps and point clouds," *Sensors*, vol. 18, no. 10, p. 3432, 2018.

[5] M. Wang, J. J. Luo, J. P. Yuan, and U. Walter, "Detumbling strategy and coordination control of kinematically redundant space robot after capturing a tumbling target," *Nonlinear Dynamics*, vol. 92, no. 3, pp. 1023–1043, 2018.

[6] Z. Ma, Y. Wang, Y. Yang, Z. Wang, L. Tang, and S. Ackland, "Reinforcement learning-based satellite attitude stabilization method for non-cooperative target capturing," *Sensors*, vol. 18, no. 12, p. 4331, 2018.

[7] C. Zagaris and M. Romano, "Reachability analysis of planar spacecraft docking with rotating body in close proximity," *Journal of Guidance, Control, and Dynamics*, vol. 41, no. 6, pp. 1416–1422, 2018.

[8] K.-B. Li, W.-S Su, and L. Chen, "Performance analysis of differential geometric guidance law against high-speed target with arbitrarily maneuvering acceleration," *Proceedings of the Institution of Mechanical Engineers, Part G: Journal of Aerospace Engineering*, vol. 233, no. 10, pp. 3547–3563, 2018.

[9] M. Ning, S. Zhang, and S. Wang, "A non-cooperative satellite feature point selection method for vision-based navigation system," *Sensors*, vol. 18, no. 3, p. 854, 2018.

[10] P. Singla, K. Subbarao, and J. L. Junkins, "Adaptive output feedback control for spacecraft rendezvous and docking under measurement uncertainty," *Journal of Guidance, Control, and Dynamics*, vol. 29, no. 4, pp. 892–902, 2006.

[11] D. Lee and G. Vukovich, "Robust adaptive terminal sliding mode control on SE (3) for autonomous spacecraft rendezvous and docking," *Nonlinear Dynamics*, vol. 83, no. 4, pp. 2263–2279, 2015.

[12] K. Xia and W. Huo, "Robust adaptive backstepping neural networks control for spacecraft rendezvous and docking with uncertainties," *Nonlinear Dynamics*, vol. 84, no. 3, pp. 1683–1695, 2016.

[13] L. Sun, W. Huo, and Z. Jiao, "Disturbance observer-based robust relative pose control for spacecraft rendezvous and proximity operations under input saturation," *IEEE Transactions on Aerospace and Electronic Systems*, vol. 54, no. 4, pp. 1605–1617, 2018.

[14] S. A. Kasaeian, N. Assadian, and M. Ebrahimi, "Sliding mode predictive guidance for terminal rendezvous in eccentric orbits," *Acta Astronautica*, vol. 140, pp. 142–155, 2017.

[15] H. Park, S. D. Cairano, and I. Kolmanovsky, "Model predictive control for spacecraft rendezvous and docking with a rotating/tumbling platform and for debris avoidance," in *Proceedings of the 2011 American Control Conference*, June-July 2011.

[16] S. Zhu, R. Sun, J. Wang et al., "Robust model predictive control for multi-step short range spacecraft rendezvous," *Advances in Space Research*, vol. 62, no. 1, pp. 111–126, 2018.

[17] H. Yan, S. Tan, and Y. Xie, "Integrated translational and rotational control for the final approach phase of rendezvous and docking," *Asian Journal of Control*, vol. 20, no. 5, pp. 1967–1978, 2018.

[18] L. Sun and Z. Zheng, "Adaptive sliding mode control of cooperative spacecraft rendezvous with coupled uncertain dynamics," *Journal of Spacecraft and Rockets*, vol. 54, no. 3, pp. 652–661, 2017.

[19] L. Sun and Z. Zheng, "Adaptive relative pose control for autonomous spacecraft rendezvous and proximity operations with thrust misalignment and model uncertainties," *Advances in Space Research*, vol. 59, no. 7, pp. 1861–1871, 2017.

[20] M. W. Harris and B. Açıkmeşe, "Minimum time rendezvous of multiple spacecraft using differential drag," *Journal of Guidance Control & Dynamics*, vol. 2, no. 2, pp. 365–373, 2014.

[21] G. Boyarko, M. O. Yakimenko, and M. Romano, "Optimal rendezvous trajectories of a controlled spacecraft and a tumbling object," *Journal of Guidance, Control, and Dynamics*, vol. 34, no. 4, pp. 1239–1252, 2011.

[22] S. Oghim, S.-H. Mok, and H. Leeghim, "Optimal spacecraft rendezvous by minimum velocity change and wait time," *Advances in Space Research*, vol. 60, no. 6, pp. 1188–1200, 2017.

[23] G. R. Duan, D. K. Gu, and B. Li, "Optimal control for final approach of rendezvous with non-cooperative target," *Pacific Journal of Optimization*, vol. 6, no. 3, pp. 521–532, 2010.

[24] M. Ciarcià, J. Ventura, M. Romano et al., "An inverse dynamics-based trajectory planner for autonomous docking to a tumbling target," in *Proceedings of the Aiaa Guidance, Navigation, & Control Conference*, San Diego, California, USA, January 2016.

[25] Y. Huang and Y. Jia, "Adaptive fixed-time relative position tracking and attitude synchronization control for non-cooperative target spacecraft fly-around mission," *Journal of the Franklin Institute*, vol. 354, no. 18, pp. 8461–8489, 2017.

[26] L. S. Breger and J. P. How, "Safe trajectories for autonomous rendezvous of spacecraft," *Journal of Guidance, Control, and Dynamics*, vol. 31, no. 5, pp. 1478–1489, 2008.

[27] S. Jacobsen, C. Lee, C. Zhu, and S. Dubowsky, "Planning of safe kinematic trajectories for free flying robots approaching an uncontrolled spinning satellite," in *Proceedings of the ASME 27th Annual Biennial Mechanisms and Robotics Conference*, American Society of Mechanical Engineers (ASME), Montreal, Canada, September-October 2002.

[28] P. Cui, T. Qin, S. Zhu, Y. Liu, R. Xu, and Z. Yu, "Trajectory curvature guidance for Mars landings in hazardous terrains," *Automatica*, vol. 93, pp. 161–171, 2018.

[29] L. Cao, D. Qiao, and J. Xu, "Suboptimal artificial potential function sliding mode control for spacecraft rendezvous with obstacle avoidance," *Acta Astronautica*, vol. 143, pp. 133–146, 2018.

[30] L. Feng, Q. Ni, Y. Bai, X. Chen, and Y. Zhao, "Optimal sliding mode control for spacecraft rendezvous with collision avoidance," in *Proceedings of the IEEE Congress on Evolutionary Computation (CEC)*, July 2016.

[31] H. Dong, Q. Hu, and M. R. Akella, "Safety control for spacecraft autonomous rendezvous and docking under motion constraints," *Journal of Guidance, Control, and Dynamics*, vol. 40, no. 7, pp. 1640–1692, 2017.

[32] H. Dong, Q. Hu, and M. R. Akella, "Dual-quaternion-based spacecraft autonomous rendezvous and docking under six-degree-of-freedom motion constraints," *Journal of Guidance, Control, and Dynamics*, vol. 41, no. 5, pp. 1150–1162, 2017.

[33] T. Chen, H. Wen, H. Hu, and D. Jin, "On-orbit assembly of a team of flexible spacecraft using potential field based method," *Acta Astronautica*, vol. 133, pp. 221–232, 2017.

[34] N. Bloise, E. Capello, M. Dentis, and E. Punta, "Obstacle avoidance with potential field applied to a rendezvous maneuver," *Applied Sciences*, vol. 7, no. 10, p. 1042, 2017.

[35] D. W. Zhang, S. M. Song, R. Pei et al., "Ellipse cissoid-based potential function guidance for autonomous rendezvous and docking with non-cooperative target," *Journal of Astronautics*, vol. 31, no. 10, pp. 2259–2268, 2010.

[36] H.-S. Shin, A. Tsourdos, and K.-B. Li, "A new three-dimensional sliding mode guidance law variation with finite time convergence," *IEEE Transactions on Aerospace and Electronic Systems*, vol. 53, no. 5, pp. 2221–2232, 2017.

[37] D. Park, H. Hoffmann, P. Pastor, and S. Schaal, "Movement reproduction and obstacle avoidance with dynamic movement primitives and potential fields," in *Proceedings of the 8th IEEE-RAS International Conference on Humanoid Robots*, pp. 91–98, Daejeon, South Korea, December 2008.

[38] S. Yang and J. Yu, "Stability analysis and variational integrator for real-time formation based on potential field," *Mathematical Problems in Engineering*, vol. 2014, Article ID 602424, 13 pages, 2014.

[39] L. T. Luh, "The shape parameter in the Gaussian function," *Computers & Mathematics with Applications*, vol. 63, no. 3, pp. 687–694, 2010.